This is the accepted manuscript (postprint) of the following article:
M. Shaker, E. Salahinejad, F. Ashtari-Mahini, *Hydrophobization of metallic surfaces by means of Al_2O_3-HDTMS coatings*, Applied Surface Science, 428 (2018) 455-462.
https://doi.org/10.1016/j.apsusc.2017.09.184

Hydrophobization of metallic surfaces by means of Al_2O_3–HDTMS coatings

M. Shaker, F. Ashtari-Mahini, E. Salahinejad *

Faculty of Materials Science and Engineering, K. N. Toosi University of Technology, Tehran, Iran

Abstract

In this work, the structure and wetting behavior of stainless steel coated with sol-gel derived alumina and hexadecyltrimethoxysilane (HDTMS) deposits were studied. As a typical result, an artificial lotus-leaf like corundum structure with a dual nano/micro-scaled roughness was developed at specific deposition and sintering conditions. Water contact angle measurements indicated that the surface functionalization by HDTMS enhances hydrophobicity, where this effect is highlighted when an alumina interlayer is used. In this regard, the most hydrophobicity level was obtained for the surface coated with the lotus-featured alumina and HDTMS coatings. In addition, using dimethylformamide contact angle measurements, the involved interfacial energies were considered to further understand and correlate the surface's roughness and wetting. In conclusion, the relatively inexpensive and facile method used in this work donates outstanding capabilities to metallic surfaces and provides a new driving force for their further developments.

Keywords: Wetting; Alumina; HDTMS; Lotus-leaf like effect

* Corresponding Author: Email Address: <salahinejad@kntu.ac.ir>

This is the accepted manuscript (postprint) of the following article:
M. Shaker, E. Salahinejad, F. Ashtari-Mahini, *Hydrophobization of metallic surfaces by means of Al_2O_3-HDTMS coatings*, Applied Surface Science, 428 (2018) 455-462.
https://doi.org/10.1016/j.apsusc.2017.09.184

1. Introduction

Surface engineering, aiming at wetting, includes versatile routes to donate especial features to the surface, such as hydrophilicity or hydrophobicity. In general, more wetting means an increase in the interaction of the substrate and a wetting liquid via providing a uniform dispersion. This characteristic considerably affects wet dependent phenomena like self-cleaning, coating, corrosion, adhesion, oil recovery, lubrication, printing and spray quenching [1-7]. In some fields like painting, coating, adhesion, printing and spraying, more hydrophilicity is favored; in contrast, fields like filtration parts, some medical devices, food processing parts and anti-corrosion species demand hydrophobicity. It would be worth mentioning that some phenomena like self-cleaning can be established with both the hydrophobic and hydrophilic features.

It is well known that the wettability of a surface is mainly controllable by surface energy and roughness, where these two essential surface characteristics establish apparent surface energy. In this regard, the decrease of surface energy and the increase of roughness enhance hydrophobicity. Typically, the application of low surface energy polymers like fluoropolymers and alkoxysilanes coatings effectively induces hydrophobicity [8-10]. However, the direct coating of alkoxysilanes like hexadecyltrimethoxysilane (HDTMS) on metals like steels does not efficiently reduce surface energy and hydrophilicity. This is because of the fact that the chemical bonding of the silane branch of alkoxysilanes with the steel surface is weak, due to the sensitivity of Fe—O—Si bond to hydrolysis [11]. Techniques including sandpapering, sandblasting, lithography, etching, electrospinning and coating can be also employed to increase roughness [12, 13]. Roughness scale and morphology strongly affect the wetting behavior, according to some experiments and models [14-16]. The roughness scale is mostly micrometers; however, when a nano-scaled roughness

This is the accepted manuscript (postprint) of the following article:
M. Shaker, E. Salahinejad, F. Ashtari-Mahini, *Hydrophobization of metallic surfaces by means of Al_2O_3-HDTMS coatings*, Applied Surface Science, 428 (2018) 455-462.
https://doi.org/10.1016/j.apsusc.2017.09.184

of suitable morphology is added, more hydrophobicity would be achieved via the creation of the lotus-leaf like effect.

There are several reports in the literature on the development of the artificial lotus-leaf like effect via methods like lithography [17], assembling carbon nanotubes [18] and nanocasting [19]. Nonetheless, most of the mentioned approaches are expensive and difficult to be controlled. Also, a number of sol-gel derived SiO_2 coatings have presented this typical feature, albeit followed by additional processes like using molds, resins, additional steps and lithography [20-23]. On the other hand, alumina (Al_2O_3) coatings are promising for different applications, due to the significant chemical stability, hardness, wear resistance, insulation and barrier properties of Al_2O_3. Concerning hydrophobization of sol-gel derived Al_2O_3 deposits, it has been reported that surface-engineered rough coatings represent a relatively low water contact angle of 32° [24]. However, to our knowledge, there is no report on the development of the lotus-leaf like effect in sol-gel derived Al_2O_3 coatings, which is achieved without any supplementary processes in the present study. Also, this research aims to improve the ineffective bonding of HDTMS to steel by using alumina interlayers. For this purpose, a range of inexpensive alumina coatings, including that exhibiting a lotus-type feature, is developed.

2. Materials and methods

In order to hydrophobize the surface of stainless steel 316, sol-gel derived alumina coatings coupled with HDTMS were employed. The materials used in this work include aluminum isopropoxide ($Al[OCH(CH_3)_2]_3$, Merck, > 98%), HDTMS ($H_3C(CH_2)_{15}Si(OCH_3)_3$, Sigma-Aldrich, > 85%), dimethylformamide ($HCON(CH_3)_2$, DAE JUNG, > 99.5%), acetic acid, nitric acid, absolute ethanol, and distilled water.

This is the accepted manuscript (postprint) of the following article:
M. Shaker, E. Salahinejad, F. Ashtari-Mahini, *Hydrophobization of metallic surfaces by means of Al_2O_3-HDTMS coatings*, Applied Surface Science, 428 (2018) 455-462.
https://doi.org/10.1016/j.apsusc.2017.09.184

For the sol-gel synthesis of alumina, 5 g aluminum isopropoxide was added to 7.4 ml ethanol at room temperature. Afterwards, 13.5 ml of distilled water and 2.8 ml of acetic acid were added to the above sol while stirring for 24 h to complete the hydrolysis and condensation reactions, making it whiter. In order to break down and peptize the synthesized alumina particle agglomerates, nitric acid was slowly added to the sol until pH of 3, leading to a clear colorless sol. Then, this sol was ultrasonicated for 10 min to further overwhelm any complex and agglomeration into smaller particles as much as possible. A part of the sol was dried at 100 °C, calcined at 500, 700 and 900 ˚C for 1 h, and then analyzed by X-ray diffraction (XRD, X'Pert Pro MPD, Cu-Kα). The other part was used for coating as follows. Polished steel substrates were rinsed in acetone, ethanol and distilled water under sonication. Then, the substrates were dipped into the prepared alumina sol at the immersion and withdrawn speeds of 90 mm/min and a dwell time of 1 min by a dip coater (Qualitech ZR-4200). The samples were dried at room temperature for 12 h and then at 100 ˚C for 1 h in an oven. Finally, they were sintered at 500, 700 and 900 ˚C for 1 h under an argon atmosphere, with the heating and cooling rates of 10 ˚C/min. This range of calcination/sintering temperature was employed to establish the suitable adhesion of the coating to the substrate (500 ˚C), to avoid the thermal deterioration of the substrate **(**900 ˚C), and to develop a range of surface morphology and roughness, which is typical for sol-gel derived films deposited on metallic substrates [25-30]. Thermogravimetric analyses on sol-gel derived alumina have confirmed the absence of any volatile species in this temperature range [31, 32], which is favorable in the preparation of sound coatings from wet sols.

A number of the uncoated and coated substrates were further processed by HDTMS coatings. To do so, 1 vol% of HDTMS was added to a solution containing ethanol and

This is the accepted manuscript (postprint) of the following article:
M. Shaker, E. Salahinejad, F. Ashtari-Mahini, *Hydrophobization of metallic surfaces by means of Al_2O_3-HDTMS coatings*, Applied Surface Science, 428 (2018) 455-462.
https://doi.org/10.1016/j.apsusc.2017.09.184

distilled water at 90:10 vol% under magnetic string. The pH value of the solution was reduced by dropwise adding acetic acid. Afterwards, the samples were placed in this solution for 1 h, dried at room temperature, and then fired at 120 ˚C for 1 h in oven to improve the chemical bonding of HDTMS to the substrate surface. The coating and sintering circumstances of the samples, with their nomination, are summarized in Table 1.

The surface and cross section of the samples were characterized by a field emission scanning electron microscope (FESEM, MIRA3 TESCAN) at the accelerating voltage of 15 kV. Also, the surface roughnesses and morphologies were further studied by an atomic force microscope (AFM, Multi-Mode Full Plus, Arapazhouhesh). The contact angles of 4 µl of water and dimethylformamide on the samples surfaces were determined by a contact angle measurement device with a repetition of 3 times. The apparent surface energy of the samples was also estimated by using the above-mentioned wetting parameters, based on the BS EN 828:2013 standard. To assess the wetting durability of the surfaces, the water contact angles were again measured after holding the samples for 6 months at room temperature under a normal radiation situation.

3. Results and discussion

Fig. 1 shows the XRD patterns of the sol-gel derived products after calcination at 500, 700 and 900 °C. As can be seen, the increase in the calcination temperature enhances the diffraction peak intensities, meaning the increase of diffusivity and thereby crystallinity. More specifically, the material calcined at 500 °C is almost amorphous albeit with a minor evidence of crystallinity. At the calcination temperature of 700 °C, more typical crystalline peaks are detected. With the more increase to 900 °C, not only the previous peaks are preserved albeit with enhanced intensities, but some new peaks also appear. According to the

This is the accepted manuscript (postprint) of the following article:
M. Shaker, E. Salahinejad, F. Ashtari-Mahini, *Hydrophobization of metallic surfaces by means of Al_2O_3-HDTMS coatings*, Applied Surface Science, 428 (2018) 455-462.
https://doi.org/10.1016/j.apsusc.2017.09.184

PANalytical X'Pert HighScore software, the crystalline phase is γ-alumina with the reference code 00-010-0425 in the International Centre for Diffraction Data (ICDD) database.

Fig. 1

Figs. 2, 3 and 4 exhibit the FESEM images of Samples 3, 5 and 7, respectively. Note that based on Table 1, the difference between the consecutive even and odd encoded samples is related to an ultrathin molecular HDTMS layer, which does not affect the surface morphology. According to Fig. 2, a uniform, continuous, dense and crack-free alumina coating with particles ranging from 20-50 nm is formed on the surface of Sample 3. Nonetheless, a number of typical cracks are observed in the low-magnification micrographs of Figs. 3 and 4, revealing a change in the surface morphology from a continuous feature (Sample 3) to micro-islands (Samples 5 and 7). The coating's shrinkage during sintering is responsible for the creation of such cracks, as accompanied by the considerable thickness of the deposited sol and the significant difference of the thermal expansion coefficient of alumina and substrate. The mean thickness of the islands for Sample 7 is estimated to be about 1 μm, based on Fig. 5. Also, the thermal expansion coefficients of alumina and austenitic stainless steel are 8 and 16 $\times$ 10^{-6}/°C, respectively [33, 34]. Although these cracks are regarded as defects in some applications like corrosion protection by coating, they frequently play a positive role in reducing wetting [12, 35] which will be proved below by the wetting probing tests. As indicated in the high-magnification FESEM images, alumina particles are uniformly accommodated on the micro-islands of Sample 5 (Fig. 3b), with the particle size of 40-80 nm which suggests the particle coarsening phenomenon in comparison to Sample 3 (Fig. 2) to reduce the apparent surface energy. In contrast, on the islands of Sample 7 (Fig. 4b), there are a number of regularly-distributed aggregations of nanoparticles with the dimensions of about 50-250 nm, which can be regarded as the lotus-leaf like effect.

This is the accepted manuscript (postprint) of the following article:
M. Shaker, E. Salahinejad, F. Ashtari-Mahini, *Hydrophobization of metallic surfaces by means of Al_2O_3-HDTMS coatings*, Applied Surface Science, 428 (2018) 455-462.
https://doi.org/10.1016/j.apsusc.2017.09.184

Fig. 2

Fig. 3

Fig. 4

Fig. 5

To interpret reasons for the creation of such a structure on Sample 7, a compromise between sintering shrinkage and particle coarsening is considered. Due to the high melting point of alumina (about 2070 °C), the sintering temperature of 500 °C (for Sample 3) is so low that the sintering process cannot considerably change the initial feature of the deposited sol. By increasing the sintering temperature, the presence of cracks infers the domination of the shrinkage of the deposited alumina layer in Samples 5 and 7. On the other hand, at the sintering temperature of 900 °C which is close to half of the alumina melting point, particle coarsening (expansion) is also activated. The interference and compromise of these local shrinkage and expansion in the coating islands, lead some particles to protrude from the upper level of the coating to reduce the strain energy, developing the lotus-leaf like effect. The appearance of holes in the vicinity of the protruding aaggregations fairly justifies this mechanism. Indeed, these holes are the previous seating of the aggregations, where the smaller volume of the holes (because of sintering shrinkage) in comparison to the adjacent expanded aggregations (caused by Ostwald ripening) is the reason for protruding of the aggregations. The creation of these aggregations has been proved both thermodynamically and empirically [36-38]. In conclusion, the appearance of the lotus-leaf like effect is determined by the following:

i) sintering temperature which controls the compromise of sintering shrinkage and coarsening,

This is the accepted manuscript (postprint) of the following article:
M. Shaker, E. Salahinejad, F. Ashtari-Mahini, *Hydrophobization of metallic surfaces by means of Al_2O_3-HDTMS coatings*, Applied Surface Science, 428 (2018) 455-462.
https://doi.org/10.1016/j.apsusc.2017.09.184

ii) thickness of the deposited layer which controls the magnitude and distribution of strain energy in the film,

iii) difference in the thermal expansion coefficient of the coating and substrate which also controls the stain energy.

The two- and three-dimensional AFM images of Samples 3, 5 and 7 are also taken to further study the surface roughness (Fig. 6). As it is evident in Fig. 6a, the surface of Sample 3 only exhibits nanometric projections which originate from alumina nanoparticles deposited on the substrate. On the surface of Sample 5, micrometric projections (equivalent to the islands characterized in the FESEM evaluations, Fig. 4) prevail over nanometric ones (Fig. 6 b). Based on Fig. 6c, nanometric projections (aggregation) appears on micron-sized islands (created by cracking in accordance to the related FESEM image, Fig. 5) for Sample 7. From the AFM studies, the roughness averages of Samples 3, 5 and 7 were also determined to be 20.6, 117.5 and 138.4 nm, respectively, indicating the increase in roughness with the sintering temperature. The considerable level of the first enhancement, with the increase of the sintering temperature from 500 °C to 700 °C, is mainly due to the development of micro-cracks in the coating, as shown above. The main difference of Samples 5 and 7 is related to the aggregations, whereas both of the samples contain cracks. In this regard, the smaller amount of the second increase in roughness, from 117.5 nm and 138.4 nm, is because of the fact that the appearance of the aggregations has a minor effect on roughness compared to micro-cracks which played a critical role in the first increase. In summary, the FESEM and AFM analyses confirm each other and will be correlated with the following wetting test results below.

Fig. 6

This is the accepted manuscript (postprint) of the following article:
M. Shaker, E. Salahinejad, F. Ashtari-Mahini, *Hydrophobization of metallic surfaces by means of Al_2O_3-HDTMS coatings*, Applied Surface Science, 428 (2018) 455-462.
https://doi.org/10.1016/j.apsusc.2017.09.184

Fig. 7 shows the macroscopic pictures of water droplets on samples' surface. The quantity of the water contact angles is also depicted in Fig. 8. Variations in the water contact angles of the surfaces after 6 month were less than 4 %, indicating the durability of the used surface-engineering processes. The increase of the contact angle by applying the HDTMS coating and by increasing the sintering temperature of the alumina coating is straightforwardly concluded. It is also noticeable that the contact angle of Sample 3 is 5° more than that of Sample 1, due to the use of the alumina coating processed at 500 °C. However, after the deposition of HDTMS, the difference in the contact angle of Samples 2 and 4 increases to 15°. This suggests that the existence of the alumina interlayer below the HDTMS coating improves the efficiency of hydrophobization. Because the chemical bonding of the silane branch of HDTMS with the steel surface is weak due to the sensitivity of Fe—O—Si bond to hydrolysis [11, 39]. Nevertheless, chemical bonding with alumina and HDTMS is resistant against hydrolysis; consequently, more effective hydrophobicity is attained [39].

Fig. 7

Fig. 8

As it is evident in Figs. 7 and 8, the application of the alumina coating processed at 500 °C, which exhibits an amorphous and flat feature, does not remarkably change the water contact angle. But when the sintering temperature is raised from 500 °C to 700 °C, a significant increase happens in the water contact angle from 34° to 90°. As signified by the XRD, FESEM and AFM analyses, it seems that the crystallization and roughening of the alumina coating, particularly the addition of micro-roughness to the nano-roughness due to cracking, contribute to an increase in hydrophobicity. The inverse relation of roughness and wetting has been reported in many publications [12, 35]. The most exciting result of this

This is the accepted manuscript (postprint) of the following article:
M. Shaker, E. Salahinejad, F. Ashtari-Mahini, *Hydrophobization of metallic surfaces by means of Al_2O_3-HDTMS coatings*, Applied Surface Science, 428 (2018) 455-462.
https://doi.org/10.1016/j.apsusc.2017.09.184

research presents itself when the sintering temperature increases to 900 °C, which corresponds to the lotus-leaf like effect. As discussed in the FESEM and AFM analyses, the lotus-leaf like effect refers to the creation of the nanometric protruding aggregations on the surface of the alumina coating, where its effect on wetting is witnessed by the increase of the water contact angle to 122° without any further surface chemical modification. Indeed, Sample 7 benefits from dual-scale roughness in both micron and nano sizes, which is regarded as the lotus-leaf like effect [14]. Many efforts have been made to develop surfaces with an inherent lotus-leaf feature, via different methods like lithography [1, 21, 22], but the method used in this research is one of the simplest approaches.

The HDTMS coating decreases wetting through reducing the surface energy caused by C—H bonds. Nonetheless, the application of the HDTMS coating is more effective on the wetting of Samples 2 and 4 than Samples 6 and 8, based on Figs. 7 and 8. The increase in the contact angle for Samples 2 and 4 is about 225 and 220 % compared to Sample 1 and 3, respectively, which is compatible to Refs. [40, 41]. In contrast, the increase for Samples 6 and 8 is 30 and 10 % compared to Samples 5 and 7, respectively, which is in agreement with Refs. [42, 43]. It can be attributed to the decrease of the contact area of the solid surface and liquid droplet for the latter samples. The Cassie-Baxter model [44] states that liquid does not penetrate into micro- and nano-cavities of a characteristic surface. Indeed, the liquid droplet on these dual-featured surfaces is in contact with two phases, the solid sample's surface and air trapped in the cavities. Thus, another difference of Sample 4 with Samples 6 and 8, in addition to the crystal structure, is related to the solid surface area fraction in contact with the liquid droplet. In this regard, the reduction of the solid surface fraction in contact with the liquid increases the contact angle through roughening surface, and albeit results to the reduction of the solid surface coated with HDTMS. However, it is concluded that the

This is the accepted manuscript (postprint) of the following article:
M. Shaker, E. Salahinejad, F. Ashtari-Mahini, *Hydrophobization of metallic surfaces by means of Al_2O_3-HDTMS coatings*, Applied Surface Science, 428 (2018) 455-462.
https://doi.org/10.1016/j.apsusc.2017.09.184

reduction of the solid surface area could not prevent HDTMS from increasing the contact angle.

The Cassie-Baxter model is applied to heterogeneous surfaces with contact angles above 90° including those developed in this work, where the Wenzel model is not applicable [45]. Heterogeneous surfaces are essentially composed of two materials, a solid material and air which are both in contact with the liquid droplet. Accordingly, Cassie-Baxter presents Eq. 1 which relates effective variables to apparent contact angle for rough and porous surfaces [44].

$$\cos\theta_m = f(\cos\theta_Y + 1) - 1 \quad (1)$$

where θ_m is the measured (apparent) contact angle, f is the fraction of solid surface in contact with the liquid and θ_Y is the ideal surface contact angle of that solid. The latter parameter refers to a flat surface without morphological factors, where its contact angle is given for different materials. This equation was used to calculate f by measuring θ_m and having θ_Y from Ref. [46], as tabulated in Table 2. The quantity f for Samples 5 and 7 is another evidence for the relation of roughness and lotus-leaf like effect. The increase of sintering temperature from 700 to 900 °C, as accompanied by the appearance of the aggregations of 50 to 250 nm in size over the alumina coating (Figs. 4 and 6), results in an enhancement in hydrophobicity through the reduction of the solid fraction in contact with the liquid.

In order to study the apparent surface energy, wetting tests with both deionized water and dimethylformamide were conducted only on Samples 2, 4, 6 and 8 which contain the HDTMS coatings, because the calculation of the apparent surface energy by the method used in this research is applicable only to low-energy surfaces like HDTMS. Because of the primary assumption of Eq. 2 (i.e. the equilibrium vapor pressure of the liquid adsorbed on the solid surface is zero), it is impossible to calculate the surface energy by measuring the contact

This is the accepted manuscript (postprint) of the following article:
M. Shaker, E. Salahinejad, F. Ashtari-Mahini, *Hydrophobization of metallic surfaces by means of Al_2O_3-HDTMS coatings*, Applied Surface Science, 428 (2018) 455-462.
https://doi.org/10.1016/j.apsusc.2017.09.184

angle of two liquids and their surface tensions for materials with high surface energy such as metals and ceramics. Based on the BS EN 828:2013 standard, in order to calculate apparent surface energy, wetting tests should be done by two liquids, one with a dominant surface tension dispersive component like dimethylformamide and the other presenting the domination of the polar component like water. Based on Figs. 9 and 10, the contact angle of dimethylformamide on Samples 2, 4 and 6 is almost the same, so that small differences may be related to measurement errors. The only difference corresponds to Sample 8 with an increased angle of about 4° than the others, which is also not a significant value. The reason behind the more wettability of the mentioned samples with dimethylformamide, in comparison to water, is "like dissolves like". In other words, the surfaces coated with HDTMS have a hydrocarbon branch which interacts with non-polar liquids like dimethylformamide, rather than with polar liquids like water having strong hydrogen bonds. Also, based on the Wenzel model [47], the low difference of the dimethylformamide contact angles on the samples' surface can be due to the fact that the dimethylformamide contact angles are very lower than 90°, where the liquid well wets the surface and penetrates into cavities and the liquid is completely in contact with HDTMS, not air. In order to determine the apparent solid surface energy components from the wetting tests of the two mentioned liquids, Eq.2 is used [48]:

$$0.5\gamma_{lg}(1+\cos\theta_Y)=\sqrt{\gamma_{sg}^{d}\gamma_{lg}^{d}}+\sqrt{\gamma_{sg}^{p}\gamma_{lg}^{p}} \qquad (2)$$

where γ_{lg} is the liquid surface tension, θ_Y is the contact angle on the ideal surface, γ_{sg}^{d} is the apparent solid surface energy dispersive component, γ_{lg}^{d} is the liquid surface energy dispersive component, γ_{sg}^{p} is the apparent solid surface energy polar component and γ_{lg}^{p} is the liquid surface energy polar component. Since there are two unknowns parameters (γ_{sg}^{d} and

This is the accepted manuscript (postprint) of the following article:
M. Shaker, E. Salahinejad, F. Ashtari-Mahini, *Hydrophobization of metallic surfaces by means of Al_2O_3-HDTMS coatings*, Applied Surface Science, 428 (2018) 455-462.
https://doi.org/10.1016/j.apsusc.2017.09.184

γ_{sg}^{p}) in Eq. 2, two different liquids with the standard conditions should be employed. The essential liquids surface tension data extracted from the literature [49] are listed in Table 3. Eventually, γ_{sg} is calculated as the sum of the apparent solid surface energy dispersive and polar components, as explained in Eq. 3. To obtain Eq. 3, it is assumed that all surface energy components except polar and dispersive ones are negligible. Also, γ_{sl} (solid-liquid interfacial tension) is calculated using the Young equation (Eq. 4).

$$\gamma_{sg}^{d} + \gamma_{sg}^{p} = \gamma_{sg} \quad (3)$$

$$\gamma_{lg}\cos\theta = \gamma_{sg} - \gamma_{sl} \quad (4)$$

Fig. 9

Fig. 10

The results of the apparent surface energy calculation are summarized in Table 4. Although the apparent solid-gas surface energy decreases by applying the different processes and coatings, the solid-liquid interfacial tension increases. Because in Eq. 4, only γ_{lg} is constant and the other parameters vary from sample to sample. It is worthy to mention that the apparent surface energy results are based on the assumption that the surface under the liquid droplet is an ideal one being composed of two phases, solid coated with HDTMS and air, which imposes some errors. As a result of these calculations, for example, the apparent solid surface energy difference of Samples 2 and 4 is based on the better chemical bonding of HDTMS with alumina in comparison to steel. Supposing that a liquid in the weightlessness condition in contact with air has a spherical shape with the contact angle of 180°, the solid surface energy based on Eqs. 2 and 3 will be zero. In other words, since there is no solid, there is no solid surface energy. Consequently, comparing Samples 6 and 8, it is concluded that the reduction of the apparent solid surface energy is due to the increase in the fraction of

This is the accepted manuscript (postprint) of the following article:
M. Shaker, E. Salahinejad, F. Ashtari-Mahini, *Hydrophobization of metallic surfaces by means of Al_2O_3-HDTMS coatings*, Applied Surface Science, 428 (2018) 455-462.
https://doi.org/10.1016/j.apsusc.2017.09.184

air in the liquid-surface interface. The increase in the air fraction from Sample 6 to 8 is due to the lotus-leaf like effect, which reveals that the addition of the 50-250 nm sized aggregations to the micro roughness results in a more contact angle caused by preventing the liquid penetration into nano/micro cavities. Solid surface energy has a significant effect on wetting, so that its reduction results in a lower tendency of the solid interaction with other materials in contact. The known value of the apparent solid surface energy enables us to predict contact angle, adhesion work and apparent interfacial energy of probing solids with liquids with the known properties, which is functional in different wetting-dependent fields. Eventually, it is anticipated that by applying the coatings developed in this work, stainless steel substrates can present additional features like waterproofing, anti-sticking, anti-contamination, self-cleaning, anti-fouling, anti-fogging and low-friction [3, 50-55].

4. Conclusion

In this research, the effect of nanoparticulate alumina and HDTMS coatings on the wetting of stainless steel was studied. The alumina coating exhibited a dense and uniform morphology while sintering at 500 °C, a dominant micro-roughness at 700 °C and the lotus-leaf like effect (hierarchical structure roughness) at 900 °C. In the coating sintered at the latter temperature, some phenomena such as cracking, particle coarsening and massive aggregations occurred, accompanied by the development of dual micro- and nano-scale roughness. Wetting studies confirmed that roughening of the surface through the coated alumina nanoparticles and lowering of the surface energy by applying the HDTMS coating had a positive effect on hydrophobicity. Furthermore, the use of the alumina interlayer coated under HDTMS led to the increase of the water contact angle. Also, the correlation among the apparent solid-gas surface energy, contact angle and low-surface energy materials/solid

This is the accepted manuscript (postprint) of the following article:
M. Shaker, E. Salahinejad, F. Ashtari-Mahini, *Hydrophobization of metallic surfaces by means of Al_2O_3-HDTMS coatings*, Applied Surface Science, 428 (2018) 455-462.
https://doi.org/10.1016/j.apsusc.2017.09.184

surfaces bonding were derived. In conclusion, it is expected that to hydrophobize surfaces via coating any material from the alkoxysilane family, nanoparticulate alumina coatings would be useful. The relatively inexpensive and facile processing method used in this study donates excellent and new capabilities to stainless steels, providing a driving force for their further practical developments.

References

1. Bhushan, B. and Y.C. Jung, *Wetting, adhesion and friction of superhydrophobic and hydrophilic leaves and fabricated micro/nanopatterned surfaces.* Journal of Physics: Condensed Matter, 2008. **20**(22): p. 225010.
2. Cole, I.S., et al., *A study of the wetting of metal surfaces in order to understand the processes controlling atmospheric corrosion.* Journal of the Electrochemical Society, 2004. **151**(12): p. B627-B635.
3. Fürstner, R., et al., *Wetting and self-cleaning properties of artificial superhydrophobic surfaces.* Langmuir, 2005. **21**(3): p. 956-961.
4. Prabhu, K.N., P. Fernades, and G. Kumar, *Effect of substrate surface roughness on wetting behaviour of vegetable oils.* Materials & Design, 2009. **30**(2): p. 297-305.
5. Zhao, X., M.J. Blunt, and J. Yao, *Pore-scale modeling: Effects of wettability on waterflood oil recovery.* Journal of Petroleum Science and Engineering, 2010. **71**(3): p. 169-178.
6. Salahinejad, E., et al., *Surface modification of stainless steel orthopedic implants by sol–gel ZrTiO4 and ZrTiO4–PMMA coatings.* Journal of biomedical nanotechnology, 2013. **9**(8): p. 1327-1335.
7. Salahinejad, E., et al., *A new double-layer sol–gel coating to improve the corrosion resistance of a medical-grade stainless steel in a simulated body fluid.* Materials Letters, 2013. **97**: p. 162-165.
8. Tshabalala, M.A., et al., *Surface chemistry and moisture sorption properties of wood coated with multifunctional alkoxysilanes by sol-gel process.* Journal of Applied Polymer Science, 2003. **88**(12): p. 2828-2841.
9. Woodward, I., et al., *Super-hydrophobic surfaces produced by plasma fluorination of polybutadiene films.* Langmuir, 2003. **19**(8): p. 3432-3438.
10. Mozafari, M., et al., *Innovative surface modification of orthopaedic implants with positive effects on wettability and in vitro anti-corrosion performance.* Surface Engineering, 2014. **30**(9): p. 688-692.
11. Huser, J., et al., *Investigation on the Adsorption of Alkoxysilanes on Stainless Steel.* Applied spectroscopy, 2013. **67**(11): p. 1308-1314.
12. Quéré, D., *Wetting and roughness.* Annu. Rev. Mater. Res., 2008. **38**: p. 71-99.
13. Shiu, J.-Y., et al., *Fabrication of tunable superhydrophobic surfaces by nanosphere lithography.* Chemistry of materials, 2004. **16**(4): p. 561-564.

14. Gao, L. and T.J. McCarthy, *The "lotus effect" explained: two reasons why two length scales of topography are important.* Langmuir, 2006. **22**(7): p. 2966-2967.
15. Cheng, Y.T., et al., *Effects of micro-and nano-structures on the self-cleaning behaviour of lotus leaves.* Nanotechnology, 2006. **17**(5): p. 1359.
16. Ranella, A., et al., *Tuning cell adhesion by controlling the roughness and wettability of 3D micro/nano silicon structures.* Acta biomaterialia, 2010. **6**(7): p. 2711-2720.
17. Bhushan, B., Y.C. Jung, and K. Koch, *Micro-, nano-and hierarchical structures for superhydrophobicity, self-cleaning and low adhesion.* Philosophical Transactions of the Royal Society of London A: Mathematical, Physical and Engineering Sciences, 2009. **367**(1894): p. 1631-1672.
18. Liu, Y., et al., *Artificial lotus leaf structures from assembling carbon nanotubes and their applications in hydrophobic textiles.* Journal of Materials chemistry, 2007. **17**(11): p. 1071-1078.
19. Sun, M., et al., *Artificial lotus leaf by nanocasting.* Langmuir, 2005. **21**(19): p. 8978-8981.
20. Wu, L.Y., et al., *Hierarchical structured sol–gel coating by laser textured template imprinting for surface superhydrophobicity.* Soft Matter, 2012. **8**(23): p. 6232-6238.
21. Manca, M., et al., *Durable superhydrophobic and antireflective surfaces by trimethylsilanized silica nanoparticles-based sol− gel processing.* Langmuir, 2009. **25**(11): p. 6357-6362.
22. Ebert, D. and B. Bhushan, *Durable Lotus-effect surfaces with hierarchical structure using micro-and nanosized hydrophobic silica particles.* Journal of colloid and interface science, 2012. **368**(1): p. 584-591.
23. Saison, T., et al., *Replication of butterfly wing and natural lotus leaf structures by nanoimprint on silica sol–gel films.* Bioinspiration & biomimetics, 2008. **3**(4): p. 046004.
24. Ruan, M., et al., *Superhydrophobic and anti-icing properties of sol–gel prepared alumina coatings.* Russian Journal of Non-Ferrous Metals, 2016. **57**(6): p. 638-645.
25. Salahinejad, E. and R. Vahedifard, *Deposition of nanodiopside coatings on metallic biomaterials to stimulate apatite-forming ability.* Materials & Design, 2017. **123**: p. 120-127.
26. Vahedifard, R. and E. Salahinejad, *Microscopic and spectroscopic evidences for multiple ion-exchange reactions controlling biomineralization of CaO. MgO. 2SiO 2 nanoceramics.* Ceramics International, 2017. **43**(11): p. 8502-8508.
27. Salahinejad, E., et al., *Influence of annealing temperature on the structural and anti-corrosion characteristics of sol–gel derived, spin-coated thin films.* Ceramics International, 2014. **40**(2): p. 2885-2890.
28. Salahinejad, E., et al., *Multilayer zirconium titanate thin films prepared by a sol–gel deposition method.* Ceramics International, 2013. **39**(2): p. 1271-1276.
29. Mozafari, M., et al., *Multilayer bioactive glass/zirconium titanate thin films in bone tissue engineering and regenerative dentistry.* International journal of nanomedicine, 2013. **8**: p. 1665.
30. Salahinejad, E., et al., *Zirconium titanate thin film prepared by an aqueous particulate sol–gel spin coating process using carboxymethyl cellulose as dispersant.* Materials Letters, 2012. **88**: p. 5-8.

This is the accepted manuscript (postprint) of the following article:
M. Shaker, E. Salahinejad, F. Ashtari-Mahini, *Hydrophobization of metallic surfaces by means of Al_2O_3-HDTMS coatings*, Applied Surface Science, 428 (2018) 455-462.
https://doi.org/10.1016/j.apsusc.2017.09.184

31. Xu, L., H. Song, and L. Chou, *Facile synthesis of nano-crystalline alpha-alumina at low temperature via an absolute ethanol sol–gel strategy.* Materials Chemistry and Physics, 2012. **132**(2): p. 1071-1076.
32. Mirjalili, F., L. Chuah, and H. Mohamad, *EFFECT OF STIRRING TIME ON SYNTHESIS OF ULTRA FINE ALPHA-Al 2 O 3 POWDER BY A SIMPLE SOL-GEL METHOD.* Journal of Ceramic Processing Research, 2011. **12**(6): p. 738-741.
33. *ASM Ready Reference: Thermal properties of metals*, ed. F. Cverna. 2002, U.S.A: ASM international.
34. Richerson, D.W., *Modern Ceramic Engineering: Properties, Processing, and Use in Design*. Third ed. 2006, U.S.A: CRC Press Taylor & Francis group.
35. Herminghaus, S., *Roughness-induced non-wetting.* EPL (Europhysics Letters), 2000. **52**(2): p. 165.
36. Rashidzadeh, M., G. Carbajal-Franco, and A. Tiburcio-Silver, *Hydrophobic coatings composed by cubic-shaped CdO nanoparticles grown by a novel and simple microwave method.* Journal of Nanoparticles, 2016. **2016**.
37. Miracle-Sole, S., *Wulff shape of crystals.* Scholarpedia, 2013. **8(10)**: p. 31266.
38. Hansen, T.W., et al., *Sintering of catalytic nanoparticles: particle migration or Ostwald ripening?* Accounts of chemical research, 2013. **46**(8): p. 1720-1730.
39. Plueddemann, E.P., *Silane coupling agents.* Additives for plastics, 1978. **1**: p. 117-119.
40. Wankhede, R.G., et al., *Development of Hydrophobic Non-Fluorine Sol-Gel Coatings on Aluminium Using Long Chain Alkyl Silane Precursor.* Journal of Materials Science and Engineering. A, 2013. **3**(4A): p. 224.
41. Arukalam, I.O., E.E. Oguzie, and Y. Li, *Fabrication of FDTS-modified PDMS-ZnO nanocomposite hydrophobic coating with anti-fouling capability for corrosion protection of Q235 steel.* Journal of colloid and interface science, 2016. **484**: p. 220-228.
42. Wang, N. and D. Xiong, *Superhydrophobic membranes on metal substrate and their corrosion protection in different corrosive media.* Applied Surface Science, 2014. **305**: p. 603-608.
43. Wang, N., et al., *Superhydrophobic surface on steel substrate and its anti-icing property in condensing conditions.* Applied Surface Science, 2015. **355**: p. 226-232.
44. Cassie, A.B.D. and S. Baxter, *Wettability of porous surfaces.* Transactions of the Faraday Society, 1944. **40**(0): p. 546-551.
45. Tuteja, A., et al., *Designing superoleophobic surfaces.* Science, 2007. **318**(5856): p. 1618-1622.
46. Zhang, D., Y. Wang, and Y. Gan, *Characterization of critically cleaned sapphire single-crystal substrates by atomic force microscopy, XPS and contact angle measurements.* Applied Surface Science, 2013. **274**: p. 405-417.
47. Wenzel, R.N., *Surface Roughness and Contact Angle.* The Journal of Physical Chemistry, 1949. **53**(9): p. 1466-1467.
48. BS.EN.828:2013, *Adhesives. Wettability. Determination by measurement of contact angle and surface free energy of solid surface.* BSI, 2013.
49. Takadoum, J., *Materials and surface engineering in tribology*. 2013: John Wiley & Sons.

This is the accepted manuscript (postprint) of the following article:
M. Shaker, E. Salahinejad, F. Ashtari-Mahini, *Hydrophobization of metallic surfaces by means of Al_2O_3-HDTMS coatings*, Applied Surface Science, 428 (2018) 455-462.
https://doi.org/10.1016/j.apsusc.2017.09.184

50. Jung, Y.C. and B. Bhushan, *Mechanically durable carbon nanotube− composite hierarchical structures with superhydrophobicity, self-cleaning, and low-drag.* ACS nano, 2009. **3**(12): p. 4155-4163.
51. Lai, Y., et al., *Transparent superhydrophobic/superhydrophilic TiO 2-based coatings for self-cleaning and anti-fogging.* Journal of Materials Chemistry, 2012. **22**(15): p. 7420-7426.
52. Zhang, H., R. Lamb, and J. Lewis, *Engineering nanoscale roughness on hydrophobic surface—preliminary assessment of fouling behaviour.* Science and Technology of Advanced Materials, 2005. **6**(3): p. 236-239.
53. Lau, K.K., et al., *Superhydrophobic carbon nanotube forests.* Nano letters, 2003. **3**(12): p. 1701-1705.
54. Wang, Z., et al., *Combined micro-/nanoscale surface roughness for enhanced hydrophobic stability in carbon nanotube arrays.* Applied physics letters, 2007. **90**(14): p. 143117.
55. Li, Y., et al., *Superhydrophobic bionic surfaces with hierarchical microsphere/SWCNT composite arrays.* Langmuir, 2007. **23**(4): p. 2169-2174.

This is the accepted manuscript (postprint) of the following article:
M. Shaker, E. Salahinejad, F. Ashtari-Mahini, *Hydrophobization of metallic surfaces by means of Al_2O_3-HDTMS coatings*, Applied Surface Science, 428 (2018) 455-462.
https://doi.org/10.1016/j.apsusc.2017.09.184

Figures

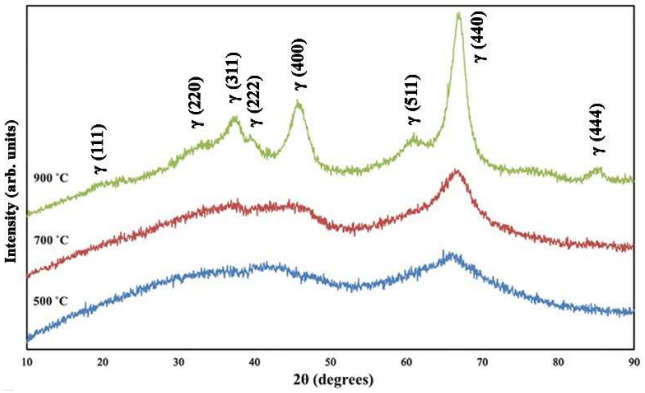

Fig. 1. XRD patterns of the sol-gel synthesized powder sample after calcination at 500, 700 and 900 °C.

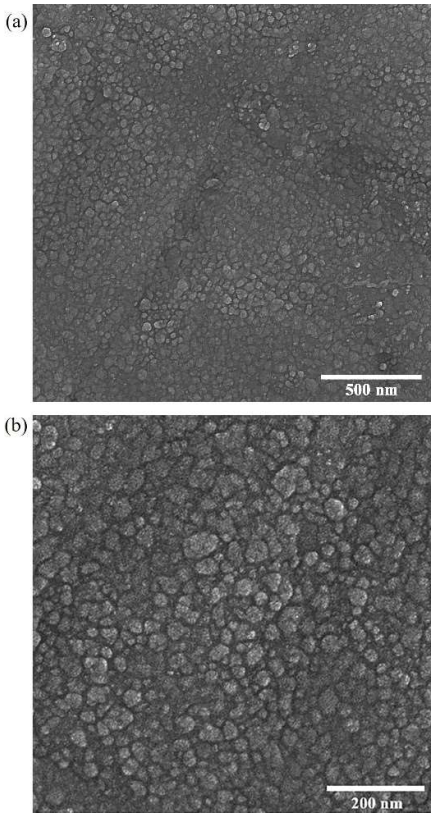

Fig. 2. FESEM micrograph taken of the surface of Sample 3 in two magnifications.

This is the accepted manuscript (postprint) of the following article:
M. Shaker, E. Salahinejad, F. Ashtari-Mahini, *Hydrophobization of metallic surfaces by means of Al_2O_3-HDTMS coatings*, Applied Surface Science, 428 (2018) 455-462.
https://doi.org/10.1016/j.apsusc.2017.09.184

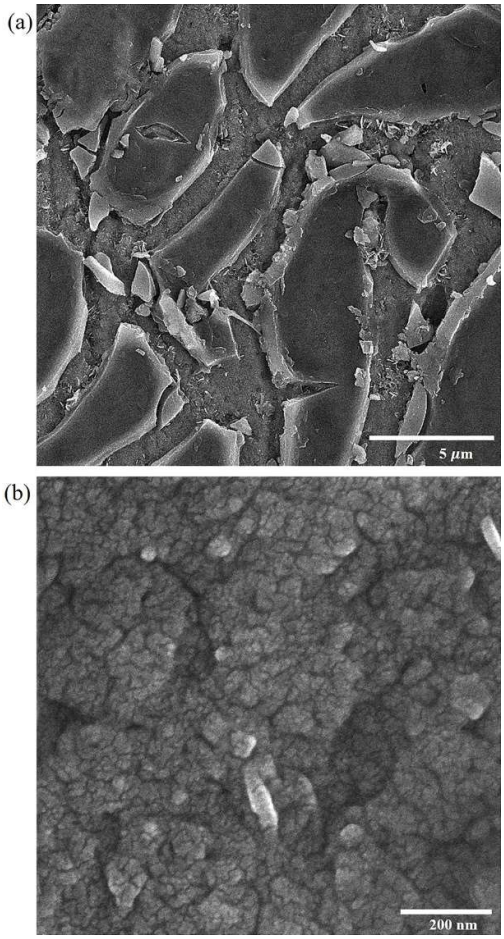

Fig. 3. FESEM micrographs taken of the surface of Sample 5 in two magnifications.

This is the accepted manuscript (postprint) of the following article:
M. Shaker, E. Salahinejad, F. Ashtari-Mahini, *Hydrophobization of metallic surfaces by means of Al_2O_3-HDTMS coatings*, Applied Surface Science, 428 (2018) 455-462.
https://doi.org/10.1016/j.apsusc.2017.09.184

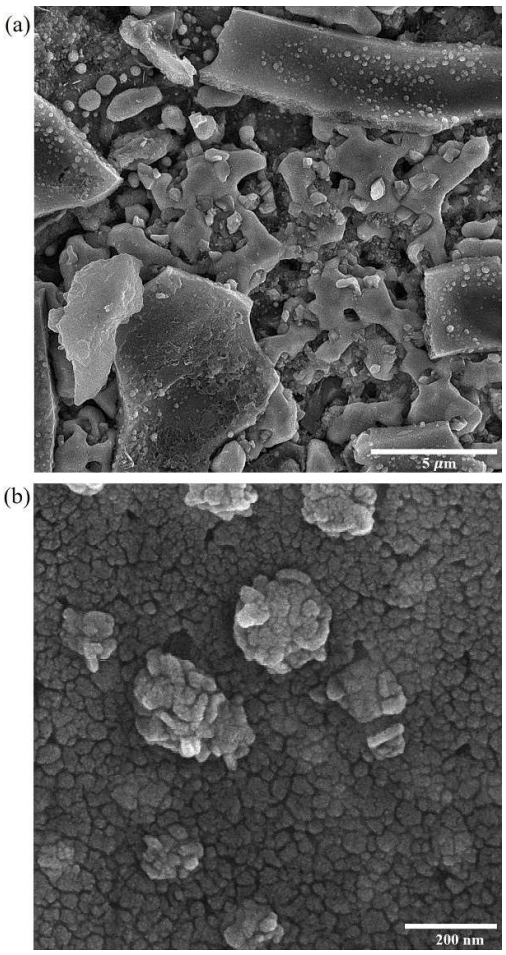

Fig. 4. FESEM micrographs taken of the surface of Sample 7 in two magnifications.

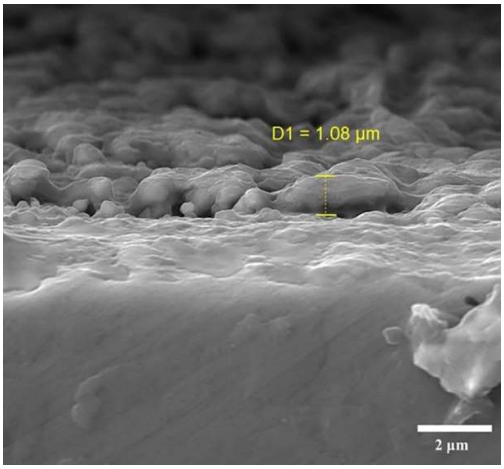

Fig. 5. FESEM micrograph taken of the cross section of Sample 7.

This is the accepted manuscript (postprint) of the following article:
M. Shaker, E. Salahinejad, F. Ashtari-Mahini, *Hydrophobization of metallic surfaces by means of Al_2O_3-HDTMS coatings*, Applied Surface Science, 428 (2018) 455-462.
https://doi.org/10.1016/j.apsusc.2017.09.184

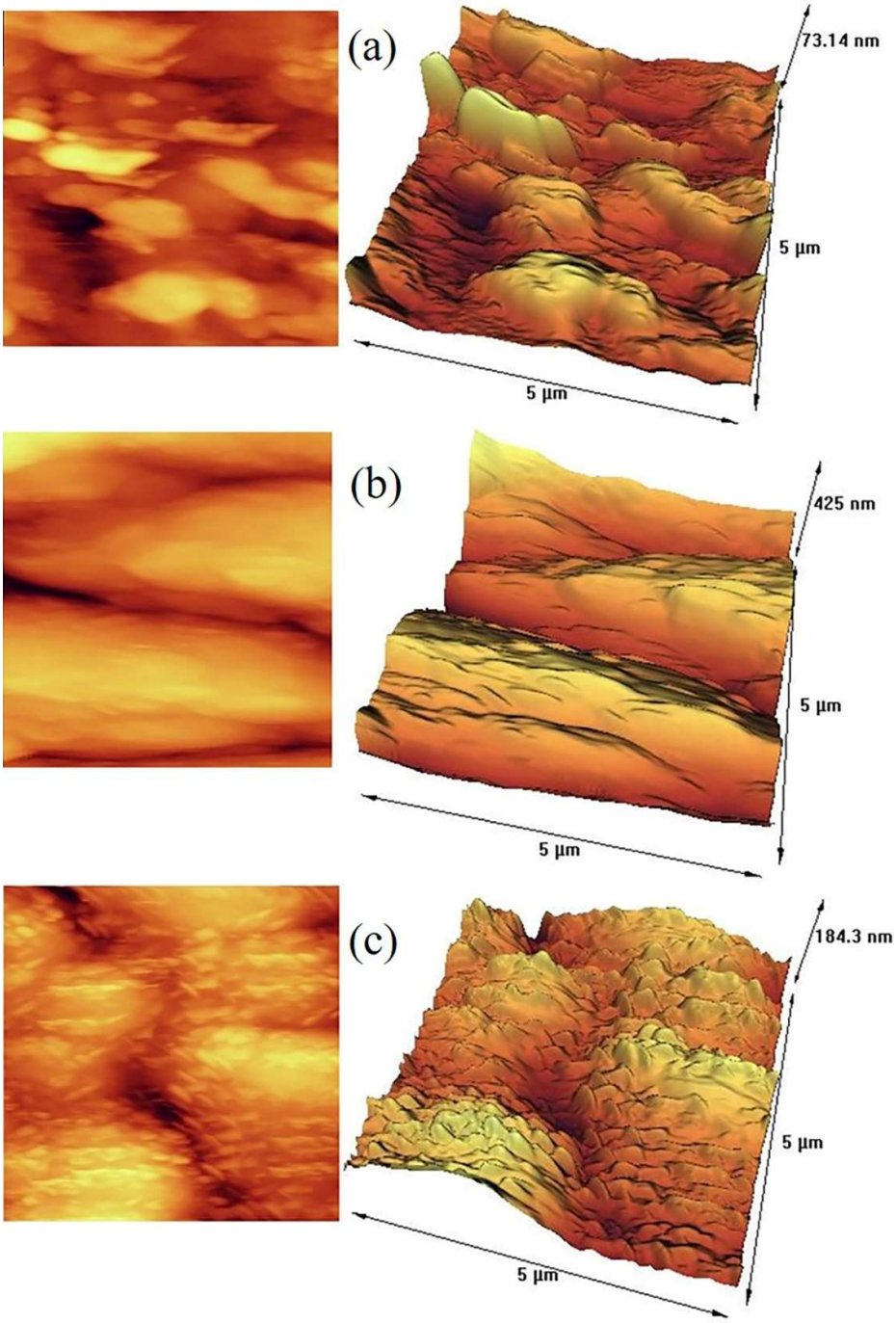

Fig. 6. Two- and three-dimensional AFM images of Samples 3 (a), 5 (b) and 7 (c).

This is the accepted manuscript (postprint) of the following article:
M. Shaker, E. Salahinejad, F. Ashtari-Mahini, *Hydrophobization of metallic surfaces by means of Al_2O_3-HDTMS coatings*, Applied Surface Science, 428 (2018) 455-462.
https://doi.org/10.1016/j.apsusc.2017.09.184

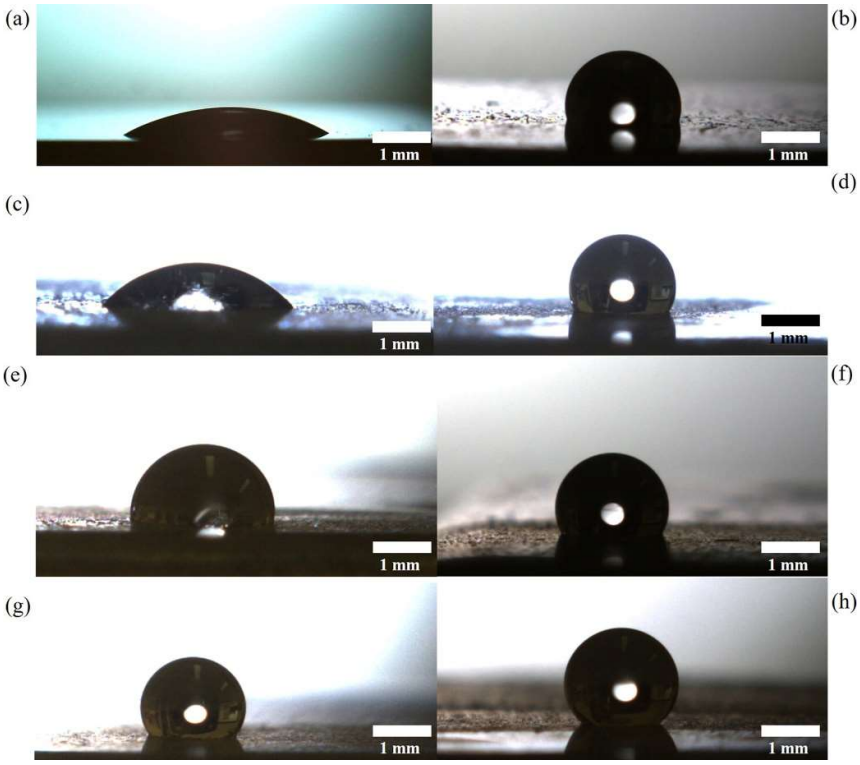

Fig. 7. Macrograph of the water droplets on the surface of Samples 1 to 8, from (a) to (h), respectively.

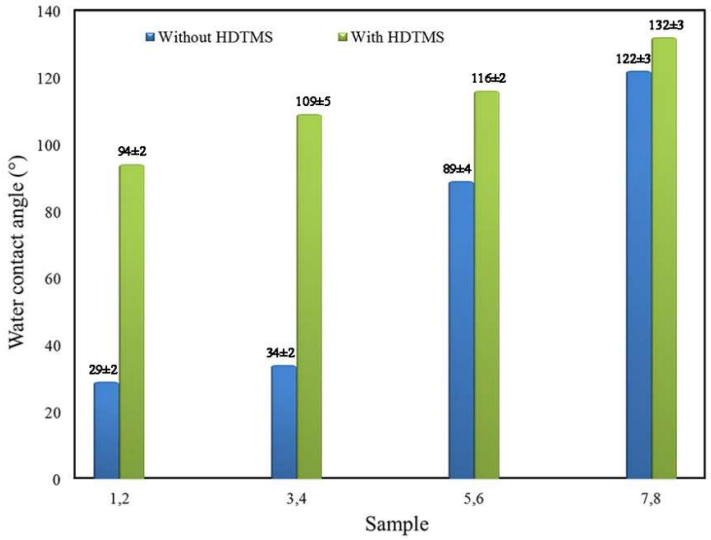

Fig. 8. Quantity of the water contact angles on the samples' surfaces.

This is the accepted manuscript (postprint) of the following article:
M. Shaker, E. Salahinejad, F. Ashtari-Mahini, *Hydrophobization of metallic surfaces by means of Al_2O_3-HDTMS coatings*, Applied Surface Science, 428 (2018) 455-462.
https://doi.org/10.1016/j.apsusc.2017.09.184

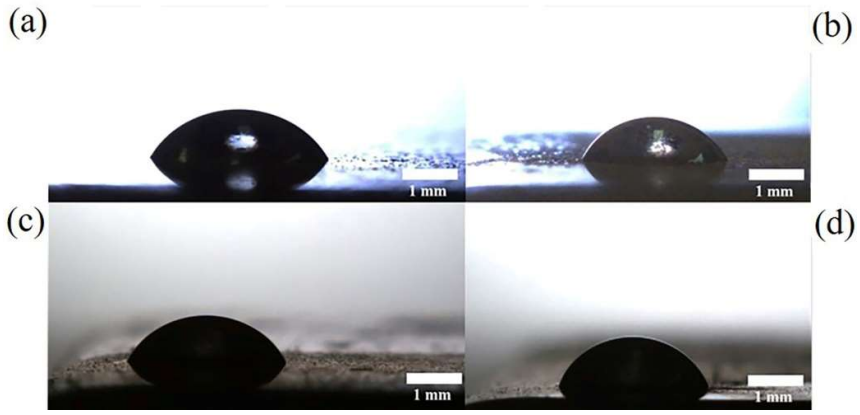

Fig. 9. Macrograph of the dimethylformamide droplets on the surface of Samples 2 (a), 4 (b), 6 (c) and 8 (d).

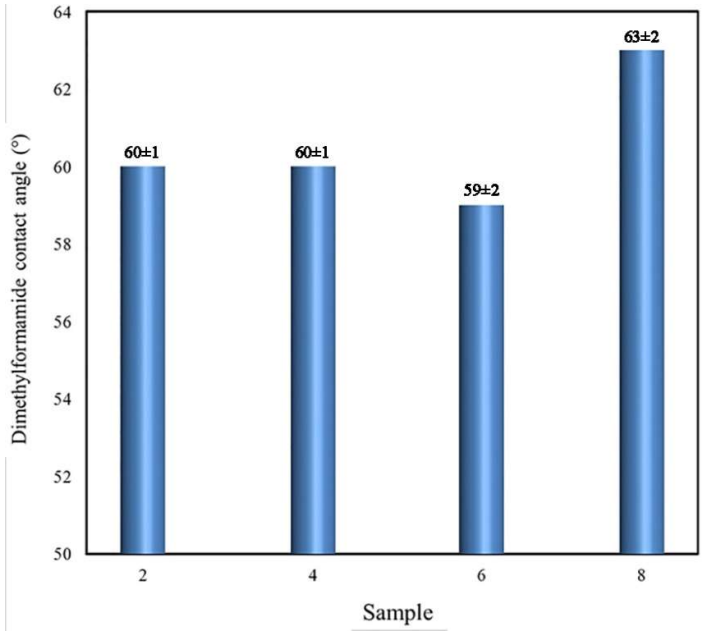

Fig. 10. Values of the dimethylformamide contact angles on the surface of Samples 2, 4, 6 and 8.

This is the accepted manuscript (postprint) of the following article:
M. Shaker, E. Salahinejad, F. Ashtari-Mahini, *Hydrophobization of metallic surfaces by means of Al_2O_3-HDTMS coatings*, Applied Surface Science, 428 (2018) 455-462.
https://doi.org/10.1016/j.apsusc.2017.09.184

Tables

Table 1. Nomination of the samples, based on the coating and sintering conditions.

Code	Sintering temperature of alumina coating (˚C)	HDTMS coating
1	-	No
2	-	Yes
3	500	No
4	500	Yes
5	700	No
6	700	Yes
7	900	No
8	900	Yes

This is the accepted manuscript (postprint) of the following article:
M. Shaker, E. Salahinejad, F. Ashtari-Mahini, *Hydrophobization of metallic surfaces by means of Al_2O_3-HDTMS coatings*, Applied Surface Science, 428 (2018) 455-462.
https://doi.org/10.1016/j.apsusc.2017.09.184

Table 2. Results of the *f* calculation based on Eq. 1.

Sample code	**Water contact angle (°)**	***f***
5	89	0.73
7	122	0.34

This is the accepted manuscript (postprint) of the following article:
M. Shaker, E. Salahinejad, F. Ashtari-Mahini, *Hydrophobization of metallic surfaces by means of Al_2O_3-HDTMS coatings*, Applied Surface Science, 428 (2018) 455-462.
https://doi.org/10.1016/j.apsusc.2017.09.184

Table 3. Essential data of the liquids' surface tension, extracted from the literature [49].

Liquid	γ_{lg} **(mN/m)**	γ_{lg}^{p} **(mN/m)**	γ_{lg}^{d} **(mN/m)**
Water	72.6	51	21.6
dimethylformamide	37.5	5	32.5

This is the accepted manuscript (postprint) of the following article:
M. Shaker, E. Salahinejad, F. Ashtari-Mahini, *Hydrophobization of metallic surfaces by means of Al_2O_3-HDTMS coatings*, Applied Surface Science, 428 (2018) 455-462.
https://doi.org/10.1016/j.apsusc.2017.09.184

Table 4. Calculated apparent surface energies.

Sample	Apparent surface energy (mN/m)			
	γ_{sg}	γ^{p}_{sg}	γ^{d}_{sg}	γ_{sl}
2	25.8	3.7	22.1	31.6
4	23.6	0.1	23.5	47.3
6	13.8	0.3	13.5	45.4
8	3.8	3.8	0.0	54.4